J. Fluid Mech. (1995), *vol.* 288, *pp.* 103–122

Near-contact electrophoretic particle motion

By MICHAEL LOEWENBERG† AND ROBERT H. DAVIS‡
Department of Chemical Engineering, University of Colorado, Boulder, CO 80309-0424, USA

(Received 22 November 1993 and in revised form 19 October 1994)

The near-contact axisymmetric electrophoretic motion of a pair of spherical particles with thin electric double layers and differing surface zeta-potentials is analysed for low Reynolds numbers and moderate surface potentials. Near-contact electrophoretic motion of a spherical particle normal to a planar conducting boundary is analysed under the same assumptions. Pairwise motion is computed by considering touching particles in point contact; relative motion is described by a perturbation about the touching state using lubrication theory. Analytical formulae are derived for two particles of disparate sizes, and for the motion of a single particle towards a boundary; numerical calculations are performed for all size ratios. The results have a universal form with respect to the particle zeta-potentials. All results indicate that the electrophoresis is a much more efficient mechanism of near-contact motion than is buoyancy. An explanation for this finding is given in terms of the electro-osmotic slip velocity on the particle surfaces that facilitates fluid removal from between approaching surfaces.

1. Introduction

Colloidal suspensions arise in a diverse range of industrial applications, particularly in biotechnology and materials processing. Predicting and manipulating the stability of a colloidal suspension is an important goal in many applications. In general, colloidal suspensions are stabilized against particle aggregation by the electric charge or ζ-potential of the suspended particles (Russel, Saville & Schowalter 1989). In an unstirred vessel, buoyancy-driven relative particle motion may result in aggregation of particles with differing sizes or densities. Charged particles migrate in an applied electric field, but, if all particles bear the same ζ-potential, their migration velocity is the same (Acrivos, Jeffrey & Saville 1990), and so there is little tendency for electrophoretic aggregation. However, in a heterogeneous suspension, electrophoretic aggregation of particles with differing ζ-potentials is possible.

Under low-Reynolds-number conditions, an isolated spherical particle sediments with its Stokes velocity through a fluid with viscosity μ (Kim & Karrila 1991):

$$U_i^{G,\infty} = \frac{2a_i^2 \Delta\rho_i}{9\mu} g, \tag{1.1}$$

where $i = 1, 2$ is the particle label, a_i is the particle radius, $\Delta\rho_i = \rho_i - \rho$ is the excess density of the particle, and g is the local acceleration due to gravity. By contrast, the

† Present address: Department of Chemical Engineering, Yale University, New Haven, Connecticut, CT 06520-2159, USA.
‡ Author to whom correspondence should be addressed.

electrophoretic velocity of a charged particle is independent of its size, shape, and density (Smoluchowski 1903):

$$U_i^{E,\infty} = \frac{\epsilon\zeta_i}{\mu} E^\infty, \tag{1.2}$$

where ϵ is the dielectric constant of the suspending fluid (usually aqueous) and E^∞ is the strength of the applied electric field.

In dilute suspensions of spherical particles, as assumed herein, aggregation rates may be predicted from pairwise calculations that require two-sphere mobility functions which describe the relative motion of two interacting spheres (Batchelor 1982). Our analysis, and the discussion that follows, are restricted to axisymmetric motions. For electrophoretic and buoyancy-driven motion, two-sphere mobility functions are efficiently approximated by the method of reflections at interparticle separations large compared to the particle sizes (Happel & Brenner 1983; Chen & Keh 1988). At separations comparable to particle size, exact solutions in bispherical coordinates are most efficient (Stimson & Jeffery 1926; Reed & Morrison 1976; Keh & Chen 1989). As the interparticle separation, h, between two particles tends to zero, relative motion parallel to their line of centres vanishes because of the large pressure required to squeeze the remaining fluid from the gap between particles. Moreover, bispherical coordinate solutions are singular for $h \to 0$. Since pairwise aggregation rates are strongly affected by particle interactions at small interparticle separations (Davis 1984; Nichols, Loewenberg & Davis 1995), an accurate description of near-contact motion is needed.

In principle, numerical boundary-collocation solutions can be used to calculate two-sphere mobility functions in the limit $h \to 0$, although these solutions are computationally intensive for small gap widths (Gluckman, Pfeffer & Weinbaum 1971; Keh & Yang 1990). Analytical, lubrication solutions are available for buoyancy-driven motion (Cooley & O'Neill 1969*a*, *b*). Generally, lubrication and series solutions overlap on a finite range of small gap widths, eliminating the need for time-consuming numerical calculations at very small gap widths.

Electrophoretic and buoyancy-driven collection rates of particles at a solid boundary from a dilute suspension can be calculated using only axisymmetric mobility functions for a single particle moving perpendicular to a planar boundary. Sphere–wall mobility functions have been derived by the method of reflections (Happel & Brenner 1983; Keh & Anderson 1985), using bispherical coordinates (Maude 1961; Brenner 1961; Keh & Lien 1989), and by collocation methods (Dagan, Pfeffer & Weinbaum 1982; Keh & Lien 1991). As for two-sphere mobility functions, method-of-reflections solutions are inaccurate, bispherical solutions become singular, and boundary collocation is time-consuming as the particle–wall separation, h, vanishes. Particle collection rates are dominated by the slow, near-contact motion of a sphere towards a solid boundary. Lubrication solutions are available for buoyancy-driven motion (Cox & Brenner 1967), but not for electrophoresis.

The aim of this paper is to provide a lubrication solution that describes the axisymmetric, near-contact electrophoretic motion of two spherical particles with radii a_1 and $a_2 = \lambda a_1$, reduced radius $a = (1/a_1 + 1/a_2)^{-1}$, and ζ-potentials ζ_1 and $\zeta_2 = \beta\zeta_1$, as depicted in figure 1. The particles are separated by a small gap width, $\delta = h/a \ll 1$, and are embedded in a uniform electric field, $\boldsymbol{E}^\infty$, parallel to their line of centres. A parallel development for buoyancy-driven, near-contact motion of two particles with excess densities $\Delta\rho_1$ and $\Delta\rho_2 = \gamma\Delta\rho_1$, is used to elucidate the fundamental differences between the two mechanisms. A lubrication formula describing near-contact electrophoretic motion of a spherical particle towards a planar conducting boundary is also presented,

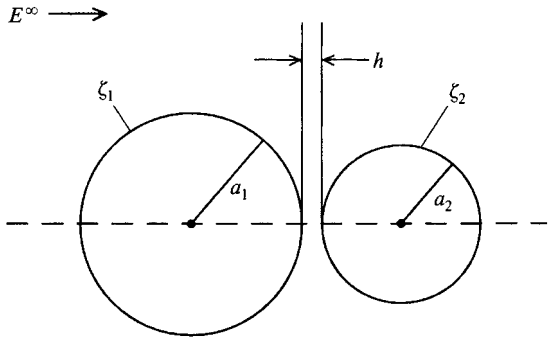

FIGURE 1. Defining sketch for two particles in close contact.

and the result is contrasted with its buoyancy-driven analogue. The results presented in this article are useful for theoretical predictions of electrophoretic aggregation and collection rates.

A detailed discussion of the assumptions appears in §2. In §3, expressions are obtained in terms of pairwise resistance functions for the relative and pair velocities of two particles that are in near contact. A scaling analysis for the two-particle lubrication problem, results for equisized particles, and an asymptotic formula for disparate particles are presented in §4. The axisymmetric electric and fluid velocity fields away from the small interparticle gap are obtained by the numerical procedure described in §5. Numerical results for pairwise and relative particle velocities are presented in §6. The related problem of a particle in near contact with a plane boundary is formulated and solved analytically in §7. Concluding remarks are made in §8.

2. Assumptions and governing equations

The analysis is restricted to moderately charged, dielectric particles with thin electric double layers (Dukhin & Derajaguin 1974; O'Brien 1983): $\kappa a_i \exp(-z|\zeta_i|/50\text{ mV}) \gg 1$, where κ^{-1} is the double-layer thickness or Debye length, and z is the valence of the highest-charged counter-ion in a room-temperature electrolyte. It can be shown that the thin-double-layer assumption is generally satisfied for moderately charged particles, $\zeta_i \sim 50$ mV, even in weak electrolytes, 10^{-4} molar or larger, provided that $a_i > 0.1$ μm (Russel *et al.* 1989).

We shall assume that the Reynolds number of particles migrating in an electric field, $Re_i^E = \rho U_i^E a_i/\mu = \rho\epsilon\zeta_i E^\infty a_i/\mu^2$, is small compared to unity. In water, $Re_i^E \sim 10^{-6}(\zeta_i/\text{mV})\,(a_i/\mu\text{m})\,(E^\infty/\text{kV m}^{-1})$, indicating that $Re_i^E \ll 1$ for $a_i < 1$ cm and typical field strengths and potentials: $E^\infty \sim 10\text{ V cm}^{-1}$ and $\zeta_i \sim 50$ mV. Brownian motion is neglected on the assumption that the Péclet number for a particle migrating in an electric field, $Pe_i^E = U_i a_i/D_i = 6\pi\epsilon\zeta_i E^\infty a_i^2/kT$, is large, where $D_i = kT/6\pi\mu a_i$ is the Stokes–Einstein particle diffusivity (Kim & Karrila 1991). In room temperature water, $Pe_i^E \sim 3(a_i/\mu\text{m})^2\,(\zeta_i/\text{mV})\,(E^\infty/\text{kV m}^{-1})$, indicating that $Pe_i^E \gg 1$ for $E^\infty \sim 10\text{ mV cm}^{-1}$, $\zeta_i \sim 50$ mV, and $a_i > 0.1$ μm. We note that non-Brownian particles typically have thin electric double layers.

The corresponding Reynolds and Péclet numbers for a particle sedimenting in room-temperature water are $Re_i^G \sim G(\Delta\rho_i/\rho)\,(a_i/30\ \mu\text{m})^3$, and $Pe_i^G \sim 10G(\Delta\rho_i/\rho)\,(a_i/\mu\text{m})^4$, where G is the local acceleration due to gravity normalized by the terrestrial value. Therefore, the assumptions $Re_i^G \ll 1$ and $Pe_i^G \gg 1$ apply for $(G\Delta\rho_i/\rho)^{-1/4}\ \mu\text{m} < a_i < 30(G\Delta\rho_i/\rho)^{-1/3}\ \mu\text{m}$, representing a size range spanning only 1–2 orders of magnitude

in normal and microgravity. By contrast, these assumptions are valid for electrophoresis of moderately charged particles in the size range $\frac{1}{10}(E^\infty/\mathrm{kV\ m^{-1}})^{-1/2}\ \mu\mathrm{m} < a_i < (E^\infty/\mathrm{kV\ m^{-1}})^{-1}\ \mathrm{cm}$, a five-orders-of-magnitude size range for $E^\infty \sim 10\ \mathrm{V\ cm^{-1}}$, provided that the suspending electrolyte is not extremely weak.

Under low-Reynolds-number conditions, fluid motion is governed by the Stokes equations (Kim & Karrila 1991). Outside the thin electric double layers on the particle surfaces, the suspending electrolyte is electrically neutral; thus, the electric field is governed by the Laplace equation (Russel *et al.* 1989). Far from the two suspended particles, we assume that the fluid is at rest and the electric field tends to the uniform value, $\boldsymbol{E}^\infty$, that is parallel to the line of centres. The electric field and fluid velocity obey

$$\boldsymbol{E}(\boldsymbol{x})\cdot\boldsymbol{n} = 0, \quad \boldsymbol{u}(\boldsymbol{x}) = \boldsymbol{U}_i - \frac{\epsilon\zeta_i}{\mu}\boldsymbol{E}(\boldsymbol{x}), \tag{2.1a,b}$$

on the particle surfaces, provided that the thin-double-layer assumption holds (Dukhin & Derajaguin 1974; O'Brien 1983). The second term on the right-hand side of (2.1*b*) represents the electro-osmotic slip velocity that results from electrically driven convection of the charged fluid in the double layer. The fluid velocity and tangential component of the electric field vanish on a conducting solid boundary.

Electrokinetic effects that arise from electric double-layer overlap between two particles in near contact are neglected, and non-hydrodynamic, colloidal forces are not included in the analysis herein. However, as discussed in the conclusion, the electrokinetic effect of double-layer overlap is easily incorporated, and colloidal forces can be combined with the results presented in this article by superposition.

3. Formulation of the two-sphere problem

3.1. *Arbitrary interparticle separations*

The theoretical description of two interacting particles in buoyancy-driven motion is reviewed first; an analogous description for electrophoretic motion follows. The force balance along the line of centres on each of two translating particles under buoyancy-driven conditions is $F_i^G + F_i^H = 0$, where $F_i^G = \frac{4}{3}\pi a_i^3 \Delta\rho_i g$ and F_i^H are the buoyancy and hydrodynamic forces, respectively, acting on each particle ($i = 1, 2$) parallel to the line of centres. By the linearity of the Stokes equations, the hydrodynamic forces may be described with hydrodynamic resistance functions:

$$F_1^H = -6\pi\mu a_1[\mathcal{A}_{12}^H(U_1 - U_2) + \mathcal{A}_{11}^H U_1], \quad F_2^H = -6\pi\mu a_1[\mathcal{A}_{21}^H(U_2 - U_1) + \mathcal{A}_{22}^H U_2], \tag{3.1}$$

where $\mathcal{A}_{11}^H \to 1$, $\mathcal{A}_{22}^H \to \lambda$, and $\mathcal{A}_{12}^H \to 0$ for widely separated, non-interacting particles, and $\mathcal{A}_{21}^H = \mathcal{A}_{12}^H$ by a Lorentz-type, reciprocal relation (Kim & Karrila 1991). The buoyancy-driven particle velocities are found by inverting these equations:

$$U_1^G = \left[\frac{1+\gamma\lambda^3}{\mathcal{A}_{11}^H + \mathcal{A}_{22}^H} + \frac{\mathcal{A}_{22}^H}{\mathcal{A}_{11}^H + \mathcal{A}_{22}^H}\frac{\mathcal{A}_{22}^H - \mathcal{A}_{11}^H\gamma\lambda^3}{\mathcal{A}_{11}^H + \mathcal{A}_{22}^H}\frac{1}{\mathcal{A}_{12}^H - \dfrac{\mathcal{A}_{11}^H\mathcal{A}_{22}^H}{\mathcal{A}_{11}^H + \mathcal{A}_{22}^H}}\right] U_1^{G,\infty}, \tag{3.2a}$$

$$U_2^G = \left[\frac{1+\gamma\lambda^3}{\mathcal{A}_{11}^H + \mathcal{A}_{22}^H} - \frac{\mathcal{A}_{11}^H}{\mathcal{A}_{11}^H + \mathcal{A}_{22}^H}\frac{\mathcal{A}_{22}^H - \mathcal{A}_{11}^H\gamma\lambda^3}{\mathcal{A}_{11}^H + \mathcal{A}_{22}^H}\frac{1}{\mathcal{A}_{12}^H - \dfrac{\mathcal{A}_{11}^H\mathcal{A}_{22}^H}{\mathcal{A}_{11}^H + \mathcal{A}_{22}^H}}\right] U_1^{G,\infty}, \tag{3.2b}$$

where $\lambda = a_2/a_1$ is the particle size ratio and $\gamma = \Delta\rho_2/\Delta\rho_1$ is the ratio of their excess densities.

Although electrophoretic motion is force free, we may consider that this results from

a balance of electro-osmotic and hydrodynamic forces: $F_i^E + F_i^H = 0$. The hydrodynamic forces, F_i^H, given by (3.1), are those acting on each of two, uncharged particles translating with velocities U_i^E. The electro-osmotic forces, F_i^E, are those required to hold stationary each of two particles that are embedded in an applied electric field, $\boldsymbol{E}^\infty$, that is parallel to their line of centres. By the linearity of the Stokes equations, the electro-osmotic forces can be expressed in terms of 'electro-osmotic resistance' functions:

$$F_1^E = 6\pi\epsilon a_1 [\Lambda_{12}^E(\zeta_1 - \zeta_2) + \Lambda_{11}^E \zeta_1] E^\infty, \quad F_2^E = 6\pi\epsilon a_1 [\Lambda_{21}^E(\zeta_2 - \zeta_1) + \Lambda_{22}^E \zeta_1] E^\infty. \quad (3.3)$$

Using (3.1), the electrophoretic migration velocity of each of a pair of force-free particles in an applied electric field is obtained:

$$U_1^E = \left[1 + (1-\beta) \left(\frac{\Lambda_{12}^E - \Lambda_{21}^E}{\Lambda_{11}^H + \Lambda_{22}^H} + \frac{\Lambda_{22}^H}{\Lambda_{11}^H + \Lambda_{22}^H} \frac{\Lambda_{12}^E \Lambda_{22}^H + \Lambda_{21}^E \Lambda_{11}^H}{\Lambda_{11}^H + \Lambda_{22}^H} \frac{1}{\Lambda_{12}^H - \dfrac{\Lambda_{11}^H \Lambda_{22}^H}{\Lambda_{11}^H + \Lambda_{22}^H}} \right) \right] U_1^{E,\infty}, \quad (3.4a)$$

$$U_2^E = \left[1 + (1-\beta) \left(\frac{\Lambda_{12}^E - \Lambda_{21}^E}{\Lambda_{11}^H + \Lambda_{22}^H} - \frac{\Lambda_{11}^H}{\Lambda_{11}^H + \Lambda_{22}^H} \frac{\Lambda_{12}^E \Lambda_{22}^H + \Lambda_{21}^E \Lambda_{11}^H}{\Lambda_{11}^H + \Lambda_{22}^H} \frac{1}{\Lambda_{12}^H - \dfrac{\Lambda_{11}^H \Lambda_{22}^H}{\Lambda_{11}^H + \Lambda_{22}^H}} \right) \right] U_1^{E,\infty}, \quad (3.4b)$$

where $\beta = \zeta_2/\zeta_1$ is the ratio of the particle zeta-potentials. We have exploited the fact that $U_1^E = U_2^E = U_1^{E,\infty}$ at all interparticle separations if $\zeta_1 = \zeta_2$ (Reed & Morrison 1976; Keh & Chen 1989), which implies that $\Lambda_{11}^E = \Lambda_{11}^H$, and $\Lambda_{22}^E = \Lambda_{22}^H$. At large interparticle separations, $\Lambda_{12}^E \to 0$, and $\Lambda_{21}^E \to \lambda$.

3.2. *Near-contact motion*

For two spherical particles in point contact ($\delta = 0$), $U_1 = U_2 = U_P$, where U_P is the pair migration velocity. In this case, the hydrodynamic resistance functions Λ_{11}^H and Λ_{22}^H are given by R_1^H and R_2^H that describe the hydrodynamic resistances of each particle for pairwise translation in the point-contact configuration. Similarly, R_1^E and R_2^E will be used to denote Λ_{12}^E and Λ_{21}^E for this tangent-sphere geometry. The hydrodynamic and electrophoretic resistance functions, Λ_{ij} $(i,j = 1,2)$, depend on size ratio and interparticle separation; the tangent-sphere resistances, R_i $(i = 1,2)$ depend only on λ.

For tangent particles, the hydrodynamic and gravity or electro-osmotic forces do not balance; a 'contact force', F_{12}, that acts on each particle with equal magnitude but opposite direction at their point of tangency completes the force balances:

$$\tfrac{4}{3}\pi a_1^3 \Delta\rho_1 g - 6\pi\mu a_1 R_1^H U_P^G - F_{12}^G = 0, \quad (3.5a)$$

$$\tfrac{4}{3}\pi a_2^3 \Delta\rho_2 g - 6\pi\mu a_1 R_2^H U_P^G + F_{12}^G = 0, \quad (3.5b)$$

$$6\pi\epsilon a_1 [R_1^E(\zeta_1 - \zeta_2) + R_1^H \zeta_1] E^\infty - 6\pi\mu a_1 R_1^H U_P^E - F_{12}^E = 0, \quad (3.6a)$$

$$6\pi\epsilon a_1 [R_2^E(\zeta_2 - \zeta_1) + R_2^H \zeta_1] E^\infty - 6\pi\mu a_1 R_2^H U_P^E + F_{12}^E = 0. \quad (3.6b)$$

Solving (3.5) and (3.6) yields the pair migration velocities and contact forces for buoyancy and electrophoretic motion:

$$U_P^G = \frac{1 + \gamma\lambda^3}{R_1^H + R_2^H} U_1^{G,\infty}, \quad U_P^E = \left[1 + (1-\beta) \frac{R_1^E - R_2^E}{R_1^H + R_2^H} \right] U_1^{E,\infty}, \quad (3.7a, b)$$

$$F_{12}^G = \tfrac{4}{3}\pi a_1^3 \Delta\rho_1 \frac{R_2^H - R_1^H \gamma\lambda^3}{R_1^H + R_2^H} g, \quad F_{12}^E = 6\pi\epsilon a_1 \zeta_1 (1-\beta) \frac{R_1^E R_2^H + R_2^E R_1^H}{R_1^H + R_2^H} E^\infty. \quad (3.8a, b)$$

It is convenient to rewrite (3.7) as

$$\frac{U_P^G}{U_1^{G,\infty}} = \frac{U_{P,1}^G}{U_1^{G,\infty}}(1+\gamma\lambda^3), \quad \frac{U_P^E}{U_1^{E,\infty}} = \frac{U_{P,1}^E}{U_1^{E,\infty}} + \beta\left(1 - \frac{U_{P,1}^E}{U_1^{E,\infty}}\right), \tag{3.9a,b}$$

where U_P/U_1^∞ is the pairwise mobility function; $U_{P,1}$ depends only on the size ratio and is the pairwise migration velocity when the smaller particle is passive (neutrally buoyant or uncharged).

Away from the gap that separates the two particles in near contact ($\delta \ll 1$), the electric field and fluid velocity can be computed to $O(\delta)$ by considering tangent particles as described above. In the gap, each field is sensitive to the gap width, but its contribution to the overall hydrodynamic and electro-osmotic resistances is very slight. In §5.4, we show that

$$\mathcal{A}_{11}^H = R_1^H + O(\delta), \quad \mathcal{A}_{22}^H = R_2^H + O(\delta), \tag{3.10a}$$

$$\mathcal{A}_{12}^E = R_1^E + O(\delta), \quad \mathcal{A}_{21}^E = R_2^E + O(\delta). \tag{3.10b}$$

Thus, the near-contact form of the individual particle velocities, given by (3.2) and (3.4), can be expressed in terms of a pair migration velocity and deviation velocities due to the contact force:

$$U_1 = U_P + \alpha U_{12}, \quad U_2 = U_P + (\alpha - 1)\, U_{12}, \tag{3.11}$$

where

$$\alpha = R_2^H/(R_1^H + R_2^H). \tag{3.12}$$

The partitioning parameter, α, describes the fraction ($0 < \alpha \leqslant \frac{1}{2}$) of the relative particle velocity, $U_{12} = U_1 - U_2$, resulting from the deviation of each particle velocity from the pair velocity attained for $\delta \to 0$:

$$U_{12} = \frac{F_{12}}{6\pi\mu a R_{12}^H}, \tag{3.13}$$

where $a = (1/a_1 + 1/a_2)^{-1}$ is the reduced radius.

The lubrication resistance, R_{12}^H, opposes the contact force, and describes the motion of two particles along their line of centres resulting from an equal-but-opposite force acting on each (Cooley & O'Neill 1969*a*):

$$R_{12}^H = \lim_{\delta \to 0} \mathcal{A}_{12}^H - \alpha R_1^H = \frac{1}{\delta} - \frac{1+7\lambda+\lambda^2}{5(1+\lambda)^2}\ln\delta + C + O(\delta \ln \delta), \tag{3.14}$$

where C is determined by matching relative particle velocities predicted by (3.13) with the results of exact calculations at small, but finite gap widths (Cooley & O'Neill 1969*a*). At leading order, (3.14) reduces to the classic Reynolds lubrication formula.

The dimensionless near-contact relative mobilities $L_{12} = U_{12}/U_{12}^\infty$ (Batchelor 1982) are obtained from (3.8), (3.13) and (3.14):

$$L_{12}^G = \frac{\delta(1+\lambda)/\lambda}{1 - \dfrac{1+7\lambda+\lambda^2}{5(1+\lambda)^2}\delta\ln\delta + C^G\delta} \frac{R_2^H - R_1^H\gamma\lambda^3}{(1-\gamma\lambda^2)(R_1^H + R_2^H)}, \tag{3.15a}$$

$$L_{12}^E = \frac{\delta(1+\lambda)/\lambda}{1 - \dfrac{1+7\lambda+\lambda^2}{5(1+\lambda)^2}\delta\ln\delta + C^E\delta} \frac{R_1^E R_2^H + R_2^E R_1^H}{R_1^H + R_2^H}, \tag{3.15b}$$

which are accurate to $O(\delta^3 \ln \delta)$. Relative mobilities are useful for trajectory calculations of pairwise aggregation rates (Davis 1984; Nichols *et al.* 1995); we can interpret L_{12} as the 'efficiency' of near-contact motion. By the invariance of particle labelling, buoyancy-driven relative particle mobilities obey the relationship $L_{12}^G(\lambda, \gamma) = L_{12}^G(\lambda^{-1}, \gamma^{-1})$; L_{12}^G is independent of the density ratio, γ, only for $\lambda = 1$ and $\gamma \neq 1$ (Batchelor 1982). In contrast, $L_{12}^E(\lambda) = L_{12}^E(\lambda^{-1})$ depends on the size ratio only (Chen & Keh 1988).

4. Scaling analysis and formulae for two particles

4.1. *Nearly equisized particles*: $1-\lambda \ll 1$

For particles of nearly equal size, the hydrodynamic and electro-osmotic resistances of each particle differ by only $O(1-\lambda)$. Thus,

$$L_{12} = O(\delta) + O(\delta[1-\lambda]), \quad \frac{U_P}{U_{EQ}} = O\left(\frac{U_1 - U_P}{U_P - U_2}\right) = 1 + O(1-\lambda), \qquad (4.1\,a,b)$$

where U_{EQ} refers to the pairwise migration velocity of an equisized pair, given by (4.2) or (4.4). For exactly equisized particles, $F_1^H = F_2^H$ and $F_1^E(\zeta_1, \zeta_2) = F_2^E(\zeta_2, \zeta_1)$ by the invariance of particle labelling. From (3.1) and (3.3), $A_{11}^H = A_{22}^H = A_{21}^E - A_{12}^E$ and $R_1^H = R_2^H = R_2^E - R_1^E$ for touching particles. According to (3.12), $\alpha = 1/2$; thus, equisized particles in electrophoretic or buoyancy motion deviate equally from the pair velocity: $U_1 - U_P = U_P - U_2$, consistent with (4.1).

From (3.7*b*), we recover the result that the electrophoretic pair migration velocity of equisized particles is exactly the average, isolated electrophoretic migration velocity of the two particles (Keh & Yang 1990):

$$U_P^E = \tfrac{1}{2}(U_1^{E,\infty} + U_2^{E,\infty}). \qquad (4.2)$$

For equisized particles, $R_1^H = R_2^H = 0.645\,141$ (Cooley & O'Neill 1969*b*); according to (3.7*a*), buoyancy-driven pair migration velocities exceed the average, isolated sedimentation velocity by 55%:

$$U_P^G = 0.775\,024(U_1^{G,\infty} + U_2^{G,\infty}). \qquad (4.3)$$

For equisized particles with different densities in near-contact buoyancy-driven motion, (3.15*a*) yields

$$L_{12}^G = \frac{\delta}{1 - \frac{9}{20}\delta \ln \delta + 1.66\delta}, \qquad (4.4)$$

where the matching constant was obtained numerically (Cooley & O'Neill 1969*a*); for $\lambda \neq 1$, the result depends on γ. The scaling prediction, (4.1*a*), indicates that electrophoretic and buoyancy-driven relative mobilities are comparable for $\lambda \approx 1$; however, quantitative results for electrophoresis reported in §6 indicate that electrophoretic relative particle motion is about three times more efficient than buoyancy for equal-size particles.

4.2. *Small size ratios*: $\lambda \ll 1$

For $\lambda \ll 1$, the buoyancy-driven flow field past a tangent pair of particles is dominated by the flow field associated with the isolated migration of the larger particle. The component of hydrodynamic stress parallel to the velocity of an isolated particle is uniform on its surface. Since the fraction of the larger particle surface occluded by the

smaller particle is $O(\lambda^2)$, we estimate that $R_1^H = 1 - O(\lambda^2)$. The hydrodynamic force on the smaller particle is estimated as $F_2^H = O[\mu a_2 u_r(\boldsymbol{x}_2)]$, where $u_r(\boldsymbol{x}_2) = O(\lambda^2 U_1^{G,\infty})$ is the radial component of the velocity field associated with the isolated, buoyancy-driven migration of the larger particle, evaluated at the centre of the smaller, tangent particle (Kim & Karrila 1991). Thus, we obtain the estimate $R_2^H = O(\lambda^3)$ for $\lambda \ll 1$; apparently, hydrodynamic and buoyancy forces on the smaller droplet are comparable.

For the case $\zeta_1 = 0$, the electro-osmotic force on the smaller particle is estimated as $F_2^E = O[\epsilon a_2 \zeta_2 E_r(\boldsymbol{x}_2)]$, where $E_r(\boldsymbol{x}_2) = O(\lambda E^\infty)$ is the radial component of the electric field evaluated at the centre of the smaller particle (Russel *et al.* 1989). According to (3.3), we obtain the estimate $R_2^E = O(\lambda^2)$ for $\lambda \ll 1$. Similarly, $R_1^E = O(\lambda^2)$ for $\lambda \ll 1$, according to (3.6*a*), (3.7*b*), (3.8*b*), and the above scaling results for R_i^H.

Inserting the above estimates into the formulae listed in §3.2, we obtain

$$\frac{U_P^E}{U_1^{E,\infty}} = 1 + O[(1-\beta)\lambda^2], \quad \frac{U_P^G}{U_1^{G,\infty}} = 1 + O(\lambda^2) + O(\gamma\lambda^3), \quad \frac{U_1 - U_P}{U_P - U_2} = O(\lambda^3) \quad (4.5a\text{–}c)$$

for $\lambda \ll 1$. These results indicate that pairwise mobilities are more sensitive to β than γ, and that the larger particle moves at nearly the pairwise velocity; relative particle motion results from the velocity deficit of the smaller particle. Most significantly, electrophoretic relative particle motion is more efficient for small size ratios:

$$L_{12}^E = O(\delta\lambda^2), \quad L_{12}^G = O(\delta\lambda^3). \quad (4.6a, b)$$

Electrophoretic motion is force-free and torque-free; thus, an isolated particle generates a potential-flow velocity field. A comparison of the potential-flow field past a spherical particle and the viscous Stokes flow field past a spherical bubble reveals that, in the neighbourhood of the sphere surface, the potential-flow field past a particle migrating with velocity $U_1^{E,\infty}$ is exactly equal to the Stokes flow field past a bubble migrating with velocity $3U_1^{E,\infty}$ (Kim & Karrila 1991). This observation implies that the electrophoretic contact force, F_{12}^E, propelling a very small, passive particle ($\zeta_2 = 0$) at the forward stagnation point of a larger, electrophoretically migrating particle equals the hydrodynamic force, F_{12}^H, that pushes a small particle towards the front stagnation point of a bubble, provided that the buoyancy-driven migration velocity of the bubble is $3U_1^{E,\infty}$. Exploiting this observation, and Takagi's (1974) solution for the hydrodynamic force on a very small particle at the stagnation point of a bubble migrating with velocity $3U_1^{E,\infty}$, we find that $F_{12}^E = F_{12}^H = 172.930\lambda^2\mu a_1 U_1^{E,\infty} = 172.930\lambda^2\epsilon a_1 \zeta_1 E^\infty$ for the case $\zeta_2 = 0$. Then, from (3.8*b*) and the fact that the resistances are independent of the zeta-potentials, we obtain $F_{12}^E = 172.930\lambda^2\epsilon a_1 \times (\zeta_1 - \zeta_2) E^\infty$ for the general case $\zeta_1, \zeta_2 \neq 0$. Inserting F_{12}^E, and the above estimates $R_2^H = O(\lambda^3)$ and $U_P^E \approx U_1^{E,\infty} = (\epsilon\zeta_1/\mu) E^\infty$ into (3.6*b*), we find that $R_2^E = 9.174\,20\lambda^2 + O(\lambda^3)$ for $\lambda \ll 1$. The analogous hydrodynamic force that pushes a very small particle towards a larger, buoyancy-driven particle is $6\pi a_1 \mu U_1^{G,\infty} R_2^H$, where $R_2^H = 4.844\,00\lambda^3 + O(\lambda^4)$ (Goren 1970). Inserting these results, and the above estimates $R_1^H \approx 1$ and $R_1^E = O(\lambda^2)$, into (3.15) and (3.12), we obtain the asymptotic formulae

$$L_{12}^E = 9.174\,20\delta\lambda^2, \quad L_{12}^G = (4.844\,00 - \gamma)\delta\lambda^3, \quad \alpha = 4.844\,00\lambda^3 \quad (4.7a\text{–}c)$$

for $\lambda \ll 1$.

4.3. *Discussion*

Electrophoresis is a much more efficient mechanism than buoyancy for near-contact relative motion between migrating particles, particularly for small size ratios. Similar observations have been made for the efficiency of thermocapillary migration of non-

conducting drops or bubbles compared to buoyancy-driven migration (Loewenberg & Davis 1993*a*). For all three mechanisms of near-contact relative particle or droplet motion, the continuous-phase fluid is forced out from the gap by a nearly constant contact force. In buoyancy-driven motion, the suspending fluid is simply squeezed out of the near-contact region by the resultant body force. For solid particles, this squeeze flow is resisted by the no-slip requirement, and so the near-contact relative motion due to buoyancy is slow.

In thermocapillary migration, a drop swims through the continuous-phase fluid because of an interfacial tension gradient that convects fluid along the drop surface from the forward to the rear stagnation point. Loewenberg & Davis (1993*a*) showed that thermocapillary near-contact relative motion of two drops is facilitated by the withdrawal of fluid from the lubrication gap because of convection along the interface of the larger, faster-moving drop. Similarly, an electrophoretically migrating particle swims through a suspending fluid because of fluid convection due to the electro-osmotic slip on its surface induced by the applied electric field. Electro-osmotic fluid withdrawal from the lubrication gap facilitates the near-contact relative motion. The enhancement is partially offset by the injection of fluids into the lubrication gap along the surface of the slower moving particle. Thus, electro-osmotic enhancement of the relative motion is most pronounced for small size ratios. However, the effect does not vanish for equisize particles, provided that $\zeta_1 \neq \zeta_2$.

5. Numerical solution for pairwise motion

5.1. *Tangent sphere coordinates*

The electric field and fluid velocity surrounding two non-conducting tangent spheres are obtained using tangent sphere coordinates (η, ν, ϕ), as depicted in figure 2. This orthogonal, right-handed coordinate system is related to a cylindrical coordinate system (z, R, θ) by (Moon & Spencer 1961)

$$z = \frac{\eta}{\eta^2+\nu^2}, \quad R = \frac{\nu}{\eta^2+\nu^2}, \quad \theta = \phi. \tag{5.1}$$

The origin is at the point of contact between the tangent spheres, and the distance from the origin is given by $r = (R^2+z^2)^{1/2} = 1/(\eta^2+\nu^2)^{1/2}$. In this coordinate system, tangent spheres of radii a_1 and a_2 with centres on the z-axis at $z = -a_1$ and $z = +a_2$ are defined by the constant coordinate surfaces $\eta = -\eta_1 = -1/2a_1$ and $\eta = \eta_2 = 1/2a_2$, respectively; the conjugate coordinate surfaces, ν = constant, are tori with zero inner radii.

5.2. *Electric field*

The electric field surrounding non-conducting particles embedded in a uniform field, $\boldsymbol{E}^\infty$, is mathematically identical to the steady-state temperature gradient field surrounding non-conducting particles embedded in a uniform temperature gradient. Thus, we obtain $E_{\nu,i}$, the tangential (ν-component) of the electric field on the surface of each sphere ($i = 1,2$; $\eta = -\eta_1, +\eta_2$) by exploiting the solution by Loewenberg & Davis (1993*a*):

$$E_{\nu,1} = -E^\infty(\eta_1^2+\nu^2)^{3/2}\int_0^\infty sP_1(s)\,J_1(s\nu)\,\mathrm{d}s, \tag{5.2a}$$

$$E_{\nu,2} = -E^\infty(\eta_2^2+\nu^2)^{3/2}\int_0^\infty sP_2(s)\,J_1(s\nu)\,\mathrm{d}s, \tag{5.2b}$$

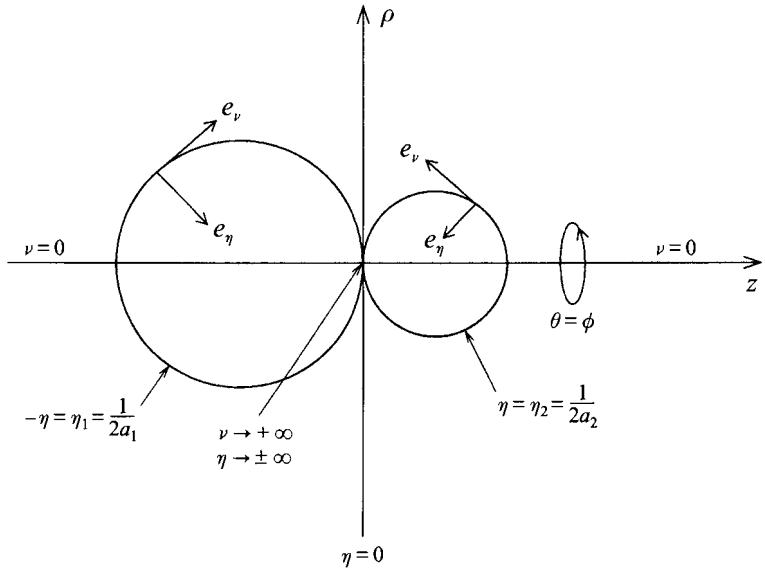

FIGURE 2. Tangent sphere coordinates for two spheres in point contact.

where $\boldsymbol{E}^\infty$ is directed in the $+z$-direction, J_1 is the first-order Bessel function of the first kind, and

$$P_1 = -\frac{s\sinh s\eta_2}{\sinh s(\eta_1+\eta_2)}, \quad P_2 = \frac{s\sinh s\eta_1}{\sinh s(\eta_1+\eta_2)}. \tag{5.3}$$

As (2.1*a*) requires, $E_\eta = 0$ on the particle surfaces: $\eta = -\eta_1, +\eta_2$. Using an identity for first-order Hankel transforms (Erdelyi *et al.* 1954), we obtain a more convenient expression to use for incorporating boundary condition (2.1*b*):

$$E_{\nu,1} = E^\infty(\eta_1^2+\nu^2)^{1/2}\int_0^\infty \left[\frac{\mathrm{d}}{\mathrm{d}s}\left(\frac{1}{s}\frac{\mathrm{d}}{\mathrm{d}s}[sP_1(s)]\right) - \eta_1^2 P_1(s)\right] sJ_1(s\nu)\,\mathrm{d}s, \tag{5.4a}$$

$$E_{\nu,2} = E^\infty(\eta_2^2+\nu^2)^{1/2}\int_0^\infty \left[\frac{\mathrm{d}}{\mathrm{d}s}\left(\frac{1}{s}\frac{\mathrm{d}}{\mathrm{d}s}[sP_2(s)]\right) - \eta_2^2 P_2(s)\right] sJ_1(s\nu)\,\mathrm{d}s. \tag{5.4b}$$

5.3. *Solution for the pairwise resistance function*

The solution for the flow fields past two touching particles is formulated using the tangent sphere coordinates described above. Under the low-Reynolds-number conditions, the axisymmetric stream function for the flow field satisfies (Kim & Karrila 1991)

$$\mathrm{E}^4\psi = 0, \tag{5.5}$$

where $\mathrm{E}^4\psi = \mathrm{E}^2(\mathrm{E}^2\psi)$ with the E^2 operator given by (Cooley & O'Neill 1969*b*):

$$\mathrm{E}^2\psi = (\eta^2+\nu^2)\left[\nu\frac{\partial}{\partial\nu}\left[\frac{1}{\nu}\frac{\partial}{\partial\nu}(\psi(\eta^2+\nu^2)^{1/2})\right] + \frac{\partial^2}{\partial\eta^2}(\psi(\eta^2+\nu^2)^{1/2})\right] = 0. \tag{5.6}$$

A general, non-singular solution of (5.5) that vanishes at infinity is (Cooley & O'Neill 1969*b*)

$$\psi = \frac{\nu}{(\eta^2+\nu^2)^{3/2}}\int_0^\infty [(A(s)+C(s)\,\eta)\sinh s\eta + (B(s)+D(s)\,\eta)\cosh s\eta]\,J_1(s\nu)\,\mathrm{d}s, \tag{5.7}$$

where $A(s)$, $B(s)$, $C(s)$ and $D(s)$ are determined from boundary condition (2.1*b*).

On the sphere surfaces, $\eta = -\eta_1, +\eta_2$, boundary condition (2.1*b*) requires that

$$\psi - \psi^{\infty} = 0, \quad \eta = -\eta_1, +\eta_2, \tag{5.8a,b}$$

$$\frac{1}{\nu}(\eta_1^2+\nu^2)^2 \frac{\partial}{\partial \eta}(\psi - \psi^{\infty})\bigg|_{\eta=-\eta_1} = -\frac{\epsilon\zeta_1}{\mu} E_{\nu,1}, \tag{5.8c}$$

$$\frac{1}{\nu}(\eta_2^2+\nu^2)^2 \frac{\partial}{\partial \eta}(\psi - \psi^{\infty})\bigg|_{\eta=\eta_2} = -\frac{\epsilon\zeta_2}{\mu} E_{\nu,2}, \tag{5.8d}$$

where $E_{\nu,1}$ and $E_{\nu,2}$ are the (tangential) electric fields on the particle surfaces, and $\psi^{\infty} = -\frac{1}{2}R^2 U_P = -\frac{1}{2}(\nu/(\eta^2+\nu^2))^2 U_P$ represents a uniform flow field in the $-z$-direction. For the present calculation, $U_1 = U_2 = U_P$ is assumed because the particles are in point contact. With the help of the identities (Erdelyi *et al.* 1954)

$$\frac{\nu}{(\eta^2+\nu^2)^{1/2}} = \int_0^{\infty} \mathrm{e}^{-s|\eta|}\left(|\eta| + \frac{1}{s}\right) J_1(s\nu)\,\mathrm{d}s, \quad \frac{\nu}{(\eta^2+\nu^2)^{3/2}} = \int_0^{\infty} \mathrm{e}^{-s|\eta|} s J_1(s\nu)\,\mathrm{d}s, \tag{5.9}$$

we obtain

$$\psi|_{\eta=-\eta_1} = -\tfrac{1}{2}U_P \frac{\nu}{(\eta_1^2+\nu^2)^{3/2}} \int_0^{\infty} \mathrm{e}^{-s\eta_1}\left(\eta_1 + \frac{1}{s}\right) J_1(s\nu)\,\mathrm{d}s, \tag{5.10a}$$

$$\psi|_{\eta=-\eta_2} = -\tfrac{1}{2}U_P \frac{\nu}{(\eta_2^2+\nu^2)^{3/2}} \int_0^{\infty} \mathrm{e}^{-s\eta_2}\left(\eta_2 + \frac{1}{s}\right) J_1(s\nu)\,\mathrm{d}s, \tag{5.10b}$$

$$\frac{1}{\nu}(\eta_1^2+\nu^2)^2 \frac{\partial\psi}{\partial\eta}\bigg|_{\eta=-\eta_1} = -2U_P \eta_1(\eta_1^2+\nu^2)^{1/2} \int_0^{\infty} \mathrm{e}^{-s\eta_1} s J_1(s\nu)\,\mathrm{d}s - \frac{\epsilon\zeta_1}{\mu} E_{\nu,1}, \tag{5.10c}$$

$$\frac{1}{\nu}(\eta_2^2+\nu^2)^2 \frac{\partial\psi}{\partial\eta}\bigg|_{\eta=\eta_2} = 2U_P \eta_2(\eta_2^2+\nu^2)^{1/2} \int_0^{\infty} e^{-s\eta_2} s J_1(s\nu)\,\mathrm{d}s - \frac{\epsilon\zeta_2}{\mu} E_{\nu,2}. \tag{5.10d}$$

Inserting the electric field solution (5.4) and stream function (5.7) into boundary conditions (5.10) yields four algebraic equations that determine $A(s) - D(s)$:

$$-A(s)\sinh s\eta_1 + B(s)\cosh s\eta_1 + C(s)\,\eta_1 \sinh s\eta_1 - D(s)\,\eta_1 \cosh s\eta_1 = -\frac{\mathrm{e}^{-s\eta_1}}{2}\left(\eta_1 + \frac{1}{s}\right) U_P, \tag{5.11a}$$

$$A(s)\sinh s\eta_2 + B(s)\cosh s\eta_2 + C(s)\,\eta_2 \sinh s\eta_2 + D(s)\,\eta_2 \cosh s\eta_2 = -\frac{\mathrm{e}^{-s\eta_2}}{2}\left(\eta_2 + \frac{1}{s}\right) U_P, \tag{5.11b}$$

$$sA(s)\cosh s\eta_1 - sB(s)\sinh s\eta_1 - C(s)\,(s\eta_1 \cosh s\eta_1 + \sinh s\eta_1) + D(s)\,(s\eta_1 \sinh s\eta_1 + \cosh s\eta_1)$$
$$= -\frac{s\eta_1 \mathrm{e}^{-s\eta_1}}{2} U_P - \left[\frac{\mathrm{d}}{\mathrm{d}s}\left(\frac{1}{s}\frac{\mathrm{d}}{\mathrm{d}s}[sP_1(s)]\right) - \eta_1^2 P_1(s)\right]\frac{\epsilon\zeta_1}{\mu} E^{\infty}, \tag{5.11c}$$

$$sA(s)\cosh s\eta_2 + sB(s)\sinh s\eta_2 + C(s)\,(s\eta_2 \cosh s\eta_2 + \sinh s\eta_2) + D(s)\,(s\eta_2 \sinh s\eta_2 + \cosh s\eta_2)$$
$$= \frac{s\eta_2 \mathrm{e}^{-s\eta_2}}{2} U_P - \left[\frac{\mathrm{d}}{\mathrm{d}s}\left(\frac{1}{s}\frac{\mathrm{d}}{\mathrm{d}s}[sP_2(s)]\right) - \eta_2^2 P_2(s)\right]\frac{\epsilon\zeta_2}{\mu} E^{\infty}, \tag{5.11d}$$

where $P_1(s)$ and $P_2(s)$ are given by (5.3). We note that the simpler forms for the electric field, (5.2*a*, *b*), are incompatible with the velocity stream function.

The forces acting on the particles are obtained by numerical integration (Cooley & O'Neill 1969*b*):

$$F_1 = 4\pi\mu a_1 \int_0^\infty s[A(s)-B(s)]\,\mathrm{d}s, \quad F_2 = -4\pi\mu a_1 \int_0^\infty s[A(s)+B(s)]\,\mathrm{d}s. \tag{5.12}$$

The results of Cooley & O'Neill (1969*b*), $F_i = -6\pi a_1 R_i^H U_P$, are recovered by setting $\zeta_1 = \zeta_2 = 0$ in (5.11). Setting $U_P = \zeta_1 = 0$ yields $F_1 = -6\pi\epsilon a_1 \zeta_2 R_1^E E^\infty$ and $F_2 = 6\pi\epsilon a_1 \zeta_2 R_2^E E^\infty$. For equisized particles in buoyancy migration, (5.11) reduces to two independent equations because of the fore-and-aft symmetry. The electrophoretic analogue is uninteresting: only the hydrodynamic resistances can be obtained for the symmetric case, $\zeta_1 = \zeta_2$, as (3.6) indicates, and the fore-and-aft symmetry for equisized particles is broken for $\zeta_1 \neq \zeta_2$.

5.4. *Velocity field near the contact point*

Demonstrating the validity of approximation (3.10) requires an analysis of the velocity field in the lubrication gap between the particles. The fluid velocity is exponentially small near the contact point between tangent spherical particles in axisymmetric, buoyancy-driven migration (Davis, *et al.* 1976; Yiantsios & Davis 1991). It follows that viscous stresses in the near-contact region between the particles make a negligible contribution to the pairwise resistance functions, Λ_{11}^H and Λ_{22}^H. Away from the gap, viscous stresses on the particle surfaces are obtained to $O(\delta)$ by the analysis presented in the preceding subsection that considers particles in point contact. Thus, (3.10*a*) is correct as asserted.

An analysis of (5.2) reveals that the axisymmetric electric field decays exponentially near the contact point between tangent spheres (Loewenberg & Davis 1993*a*). With the help of boundary condition (2.1*b*), and the results for buoyancy-driven migration, we conclude that the velocity field is exponentially small near the contact point between tangent spherical particles in axisymmetric, electrophoretic migration. Then, by the arguments used above for buoyancy-driven migration, we conclude that (3.10*b*) is also valid. For both electrophoretic and buoyancy-driven migration, the flow field in the near-contact region is dominated by the lubrication flow associated with the relative motion between two spherical particles under the action of a constant force, F_{12}.

6. Numerical results and discussion

6.1. *Pairwise mobilities*

As is apparent from (3.9), electrophoretic and buoyancy-driven pairwise mobilities for all density, charge, and size ratios can be inferred from the function $U_{P,1}$, which depends only on the size ratio and is shown in figure 3. As an illustrative example, consider two particles with size, charge, and density ratios given by $\lambda = \beta = 0.5$ and $\gamma = 0$. From figure 3, we find that $U_{P,1}^E/U_1^{E,\infty} = 0.842$ and $U_{P,1}^G/U_1^{G,\infty} = 0.953$; then, from (3.9), we obtain $U_P^E/U_1^{E,\infty} = 0.921$ and $U_P^G/U_1^{G,\infty} = 0.953$. Equation (3.9*b*) indicates that electrophoretic pairwise mobilities exceed the isolated mobility of the larger particle if, and only if, $\beta > 1$. Equation (3.9*a*) and the results depicted in figure 3 imply that $U_P^G > U_1^{G,\infty}$ can occur for $\gamma < 1$. Pairwise electrophoretic mobilities vanish for $\beta = -(U_{P,1}^E/U_1^{E,\infty})/(1-U_{P,1}^E/U_1^{E,\infty})$, whereas $\gamma = -\lambda^{-3}$ yields $U_P^G = 0$. As (4.5) predicts, figure 3 and (3.9) indicate that β and γ have comparable effects on pair mobilities for $\lambda = O(1)$; however, U_P^E is much more sensitive to β than U_P^G is to γ for $\lambda \ll 1$.

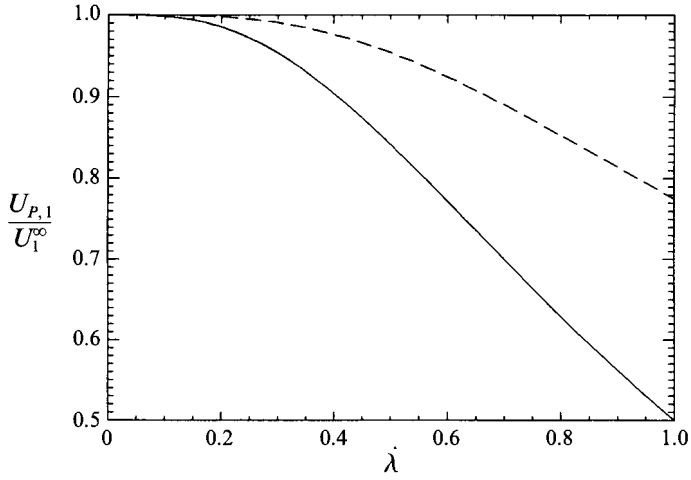

FIGURE 3. Electrophoretic (solid curve, $\beta = 0$) and buoyancy (dashed curve, $\gamma = 0$) pair mobilities versus particle radius ratio. Results for β, $\gamma \neq 0$ are obtained from equation (3.9).

6.2. *Relative mobilities*

At leading order,

$$L_{12}\delta^{-1} = \frac{F_{12}}{6\pi\mu a U_{12}^\infty}, \tag{6.1}$$

according to (3.13) and (3.14). Figure 4 depicts $L_{12}\delta^{-1}$ as a function of size ratio. As discussed beneath (3.15), electrophoretic relative mobilities are fully conveyed by these results. Buoyancy-driven relative mobilities depend also on γ. We chose $\gamma = 0$ for comparing the two mechanisms; similar results were obtained for different values. Also shown in figure 4 is the relative motion partitioning coefficient, as defined by (3.11) and (3.12); individual particle velocities can, therefore, be inferred from figures 3 and 4. For example, consider two particles with size, charge, and density ratios given by $\lambda = \beta = 0.5$ and $\gamma = 0$. From figure 4, we find that $L_{12}^E\delta^{-1} = 2.59$, $L_{12}^G\delta^{-1} = 0.532$, and $\alpha = 0.179$. Then, from (3.11) and the pairwise velocities calculated above, we obtain $U_1^E/U_1^{E,\infty} = 1.38$, $U_2^E/U_1^{E,\infty} = 1.21$, $U_1^G/U_1^{G,\infty} = 1.05$, and $U_2^G/U_1^{G,\infty} = 0.52$.

The efficiency of electrophoretic relative motion, compared to buoyancy-driven relative motion, is illustrated in figure 5. Apparently, $L_{12}^E/L_{12}^G > 3$ for all size ratios, and $L_{12}^E/L_{12}^G \approx 1.89/\lambda(1-0.206\gamma)$ for $\lambda \ll 1$, as predicted by (4.7*a*, *b*).

Figure 6 depicts relative mobilities as a function of gap width. The complete lubrication solution, (3.15), is contrasted with the leading-order approximation, (6.1); the required parameters are listed in table 1. Also shown are exact calculations obtained using the collocation solution for electrophoretic motion by Keh & Yang (1990), who generously supplied their FORTRAN algorithm, and a bispherical coordinate solution (Stimson & Jeffery 1926) for buoyancy motion. The results depicted in figure 6 demonstrate that the complete and leading-order lubrication solutions converge to the exact results in the limit $\delta \to 0$, and that the complete lubrication solution accurately approximates exact calculations at even moderate gap widths.

For buoyancy-driven particle motion, the exact, bispherical coordinate solution converged at all gap widths in the range depicted in figure 6. For electrophoretic migration, Keh & Yang's (1990) collocation algorithm was implemented using $N_T = N_1 + N_2 \leqslant 240$ total collocation points, where $N_1/N_2 = \lambda$, and $N_i (i = 1, 2)$ are the

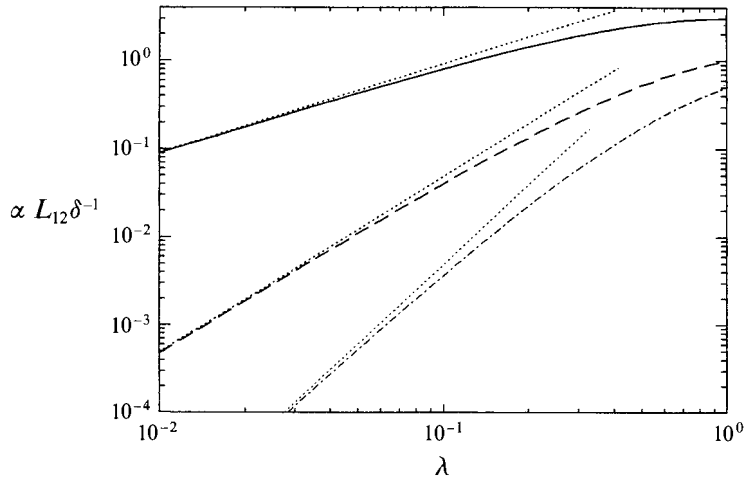

FIGURE 4. Electrophoretic (solid curve) and buoyancy-driven (dashed curve, $\gamma = 0$) relative particle mobilities and partitioning parameter (dashed-dotted curve) versus particle radius ratio; the dotted lines represent asymptotic formulae (4.7) for small size ratios.

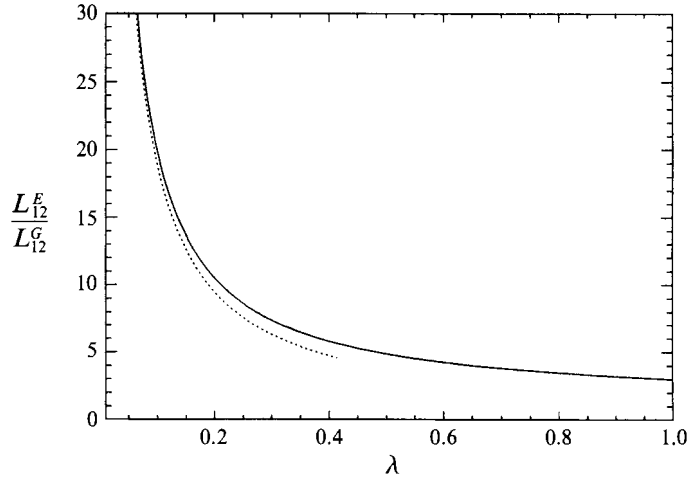

FIGURE 5. Ratio of electrophoretic to buoyancy-driven ($\gamma = 0$) relative particle mobilities versus particle radius ratio; the dotted curve represents asymptotic formulae (4.7) for small size ratios.

collocation points on each particle. With this policy, the collocation algorithm successfully converged for all calculated results depicted in figure 6; convergence was not achieved at smaller gap widths. The results indicate that the performance of the collocation solution deteriorates as the particle size ratio decreases; using $N_T \leqslant 240$, it was not possible to determine the matching constant for $\lambda < \frac{1}{4}$ by the procedure described beneath (3.14). In principle, numerical convergence could have been achieved at smaller gap widths, and for smaller size ratios, by increasing N_T; however, implementing the collocation algorithm with $N_T > 240$ is time consuming. Moreover, the performance of the collocation algorithm (Keh & Yang 1990) is superior (Keh, personal communication) to an exact solution is bispherical coordinates (Keh & Chen, 1989). These observations provide practical motivation for the lubrication solutions presented in this article.

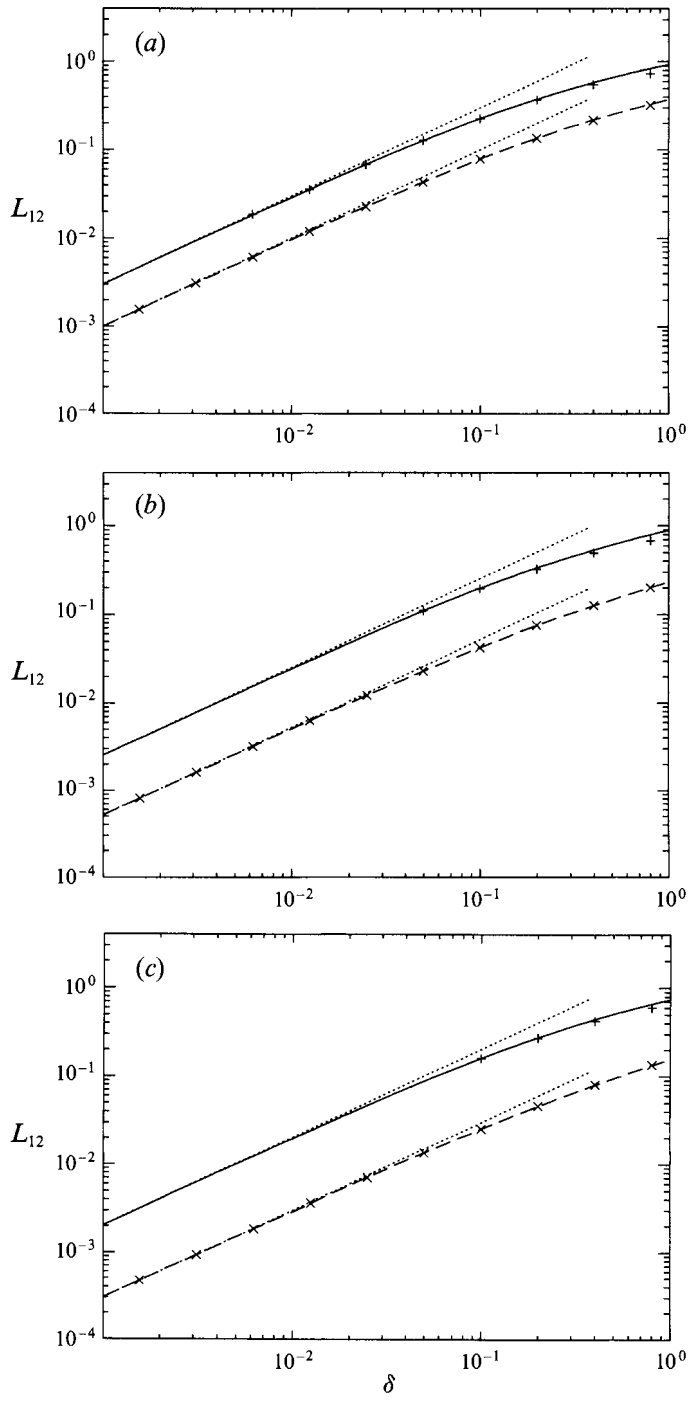

FIGURE 6. Higher-order solution for electrophoretic (solid curves) and buoyancy-driven (dashed curves; $\gamma = 0$) relative particle mobilities versus dimensionless separation for size ratios (*a*) $\lambda = 1$, (*b*) $\lambda = 1/2$, and (*c*) $\lambda = 1/3$. The dotted lines are the leading-order solutions from (4.7); the symbols represent exact calculations for electrophoresis from Keh & Yang's (1990) collocation algorithm (+) and a bispherical coordinate solution for buoyancy-driven motion (×).

λ	1	1/2	1/3	1/4	1/5	1.10
$L_{12}^E\delta^{-1}$	3.01105	2.53644	2.02634	1.66840	1.41403	0.798428
C^E	2.24	1.84	1.71	≈ 1.5	(−)	(−)

TABLE 1. Values for the electro-osmotic 'contact force', and matching constant in (3.13) and (3.14) that were obtained according to the numerical procedure described in §5; (−) indicates that the matching constant could not be evaluated from exact calculations using $N_T = 240$ collocation point. The asymptotic formula, (4.7*a*), is accurate to 5% for $\lambda \leqslant 1/30$.

7. Motion of a particle towards a planar boundary

In this section, we determine the motion of a charged spherical particle towards a nearby conducting boundary due to an applied electric field, $\boldsymbol{E}^\infty$, normal to the boundary. The lubrication solution contained herein complements the collocation solution of the same problem presented by Keh & Lien (1991). We note, however, that the normal electric field will cause a flow of ionic charge toward the boundary; the ionic species build up near the boundary and cancel the electric field in the vicinity of the boundary after a short time. This electrode polarization limits the practical application of the results.

By analogy with the development in §3, we write

$$U_B = \frac{F_B}{6\pi\mu a R_B}, \tag{7.1}$$

where U_B is the near-contact velocity of a particle with radius a normal to the planar boundary, F_B is a constant, or nearly constant, contact force that drives the particle towards the boundary, and R_B is the lubrication resistance given by (3.14) in the limit $\lambda \to 0$. Taking $F_B^G = \frac{4}{3}\pi a^3 \Delta\rho g$, Cox & Brenner (1967) obtained

$$L_B^G = \frac{\delta}{1 - \frac{1}{5}\delta\ln\delta - 0.028\,720\delta} \tag{7.2}$$

for gravity-driven motion with $\delta = h/a \ll 1$, where the matching constant in (3.14) was determined analytically (Maude 1961; Brenner 1961). $L_B = U/U^\infty$ defines the sphere–boundary mobility function, where U^∞ is given by (1.1) or (1.2).

By analogy with (7.2), the electro-osmotic force acting on a stationary particle at arbitrary particle–wall separations is $F_B^E = 6\pi\epsilon a\zeta \Lambda_B^E E^\infty$, where Λ_B^E is the electro-osmotic resistance. For $\delta = 0$, $\Lambda_B^E = R_B^E$, where R_B^E is the electro-osmotic resistance for a particle touching a planar conducting boundary. It will be shown that the electric field and fluid velocity in the near-contact region make a negligible contribution to Λ_B^E:

$$\Lambda_B^E = R_B^E + O(\delta). \tag{7.3}$$

With the help of (7.1), we obtain the electrophoretic analogue of (7.2), representing the sphere–boundary analogue of (3.15*b*):

$$L_B^E = \frac{\delta}{1 - \frac{1}{5}\delta\ln\delta + C^E\delta} R_B^E. \tag{7.4}$$

Away from the near-contact region, the electric field strength and the resulting electro-osmotic flow field on the particle surface are comparable to those on an isolated particle; it follows that $R_B^E = O(1)$. Thus, with the help of (7.2) and (7.4), we obtain the estimate $L_B = O(\delta)$ for both electrophoretic and buoyancy-driven, near-contact

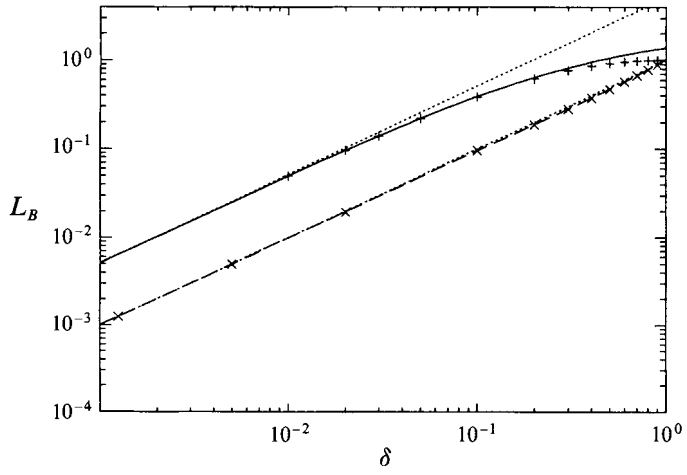

FIGURE 7. Higher-order solution for electrophoretic (solid curves) and buoyancy-driven (dashed curves) particle–boundary mobilities versus dimensionless separation. The dotted lines are the leading-order solutions; + and × represent exact calculations for electrophoresis (Keh & Lien 1991) and buoyancy-driven motion (Cooley & O'Neill 1969*a*), respectively.

particle motion towards a boundary. According to an analysis similar to that presented by Loewenberg & Davis (1993*b*) for the thermocapillary motion of a drop near a plane,

$$R_B^E = \int_0^\infty \frac{\frac{2}{3}s+\frac{1}{2}\sinh 2s}{\sinh^2 s - s^2}\frac{\sinh s}{\cosh^3 s}s^2\,\mathrm{d}s = 5.13817. \tag{7.5}$$

Inserting this result into (7.4), we obtain

$$L_B^E = \frac{5.13817\delta}{1-\frac{1}{5}\delta\ln\delta+2.71\delta}, \tag{7.6}$$

where the matching constant, C^E, was obtained by the procedure described beneath (3.14) using the exact results of Keh & Lien (1991).

Figure 7 depicts sphere–boundary mobilities as a function of gap width. The lubrication solutions, (7.2) and (7.6), are compared to exact calculations for electrophoretic (Keh & Lien 1991) and buoyancy-driven (Cooley & O'Neill 1969*a*) motion of a particle towards a planar boundary. The results indicate that the lubrication solutions, and their $O(\delta)$ approximations, converge to the exact results for $\delta \to 0$.

Keh & Lien (1991) report exact results, obtained using boundary collocation, for $\delta \geqslant 0.01$. Presumably, results for smaller gap widths could have been obtained by increasing the number of collocation points, but this is a time-consuming procedure. By contrast, Cooley & O'Neill report exact calculations, obtained using a bispherical coordinate solution, for exceedingly small gap widths: $\delta \geqslant 5\times10^{-5}$. The difficulty of obtaining exact results for near-contact electrophoretic motion indicates the need for the lubrication solutions presented in this paper, as noted at the end of §6.2.

The lubrication formulae, (7.2) and (7.6), and the results depicted in figure 7, indicate that near-contact electrophoresis towards a planar boundary is about five times more efficient than buoyancy-driven motion. Similarly, near-contact thermocapillary migration of a bubble towards a conducting, solid boundary is about twice as efficient as buoyancy-driven migration (Loewenberg & Davis 1993*b*). The results obtained in this section apparently generalize the analogy between electrophoretic

and thermocapillary near-contact motion, discussed in §4.3. For both mechanisms, near-contact motion is enhanced relative to buoyancy-driven motion by a net thermocapillary or electro-osmotic withdrawal of continuous-phase fluid from the lubrication gap.

8. Concluding remarks

In this work, we have analysed axisymmetric, near-contact electrophoretic particle motion. We considered pairwise and relative motion between a pair of migrating particles, and the near-contact motion of a charged particle towards a conducting planar boundary. Simple expressions were obtained that describe electrophoresis normal to a boundary, and the relative electrophoretic motion between a pair of particles that are very different in size. Numerical calculations were performed for all size ratios.

Throughout the article, the results for electrophoretic motion are contrasted with those for buoyancy-driven motion. The results for electrophoresis have a universal form with respect to the ratio of ζ-potentials; they depend only on size ratio, $0 < \lambda \leqslant 1$. Buoyancy-driven relative mobilities depend on size and density ratios. Near-contact electrophoretic interparticle motion is at least three times more efficient than buoyancy-driven motion; an asymptotic formula indicates that electrophoresis is a much more efficient mechanism of near-contact relative motion for small particle size ratios. An analytical solution indicates that near-contact electrophoretic migration of a particle towards a boundary is approximately five time more efficient than buoyancy-driven motion.

Exact calculations of near-contact electrophoretic motion were found to be computationally intensive at small gap widths. This suggests that the two-particle lubrication solution formulated in this article will be particularly helpful for obtaining the accurate near-contact relative mobilities that are needed for calculating electrically driven aggregation rates. Similarly, the formula for near-contact electrophoretic motion towards a boundary is needed for calculating the rate of electrophoretic particle collection at a conducting boundary.

An analogy between near-contact thermocapillary migration of non-conducting drops and electrophoresis of charged particles is discussed; both mechanisms of near-contact motion are considerably more efficient than buoyancy. A qualitative explanation for this observation involves withdrawal of the continuous-phase fluid from the near-contact region by electro-osmotic or interfacial-tension-driven surface convection. For all three mechanisms, pairwise and relative particle motions can be decoupled; near-contact motion is driven by a nearly constant 'contact force'.

Electrokinetic effects associated with electric double-layer overlap may be incorporated into the leading-order solution for near-contact particle motion, developed herein, by using the electrohydrodynamic lubrication formula of Bike & Prieve (1990):

$$R_{12}^{EH} = \frac{1}{\delta}\left[1 + B\left(\frac{1+\beta}{\delta\kappa a}\right)^2 + O\left(\frac{1+\beta}{\delta\kappa a}\right)^4\right], \tag{8.1}$$

for thin, slightly overlapping double layers, $\delta\kappa a \gg 1$. In a room-temperature electrolyte, $B \approx 4\times 10^{-5}(\zeta_1/\mathrm{mV})^2$, so that $B \sim 0.1$ for $\zeta_1 \sim 50$ mV. The electrokinetic effect of overlapping double layers is incorporated by inserting (8.1) into (3.13); thus, (6.1) becomes

$$L_{12} = \frac{F_{12}}{6\pi\mu a U_{12}^{\infty}} \frac{\delta}{1 + B(1+\beta/(\delta\kappa a))^2}, \tag{8.2}$$

for electrophoretic and buoyancy-driven near-contact particle motion, where F_{12} is obtained in this article. Apparently, electrohydrodynamic effects are unimportant for $\delta\kappa\alpha \gg B^{1/2}$. Formula (8.1), and the result (8.2), are restriction to $\delta\kappa a \gg 1$. A generalization of (8.1), valued for $\delta\kappa\alpha \leqslant O(1)$, is at present unavailable; the effect of electrohydrodynamic lubrication for significantly overlapping double layers is generally dominated by the hydrodynamic lubrication resistance considered herein (S. G. Bike, personal communication). For near-contact particle motion towards a plane boundary, a result similar to (8.2) is obtained using (7.1); the result is subject to the same restriction $\delta\kappa\alpha \gg 1$.

Finally, we note that non-hydrodynamic, colloidal forces are readily incorporated into the analysis developed herein by writing (Batchelor 1982)

$$\frac{U_{12}}{U_{12}^{\infty}} = \pm L_{12} - \frac{F_{VDW} - F_{ESR}}{R_{12}\, U_{12}^{\infty}}, \tag{8.3}$$

for near-contact relative motion along the line of centres between a pair of migrating particles, where the + or − sign is taken depending on whether the near contact tends to increase or decrease the interparticle separation; F_{VDW} and F_{ESR} represent the van der Waals attractive and electrostatic repulsive forces, respectively. A similar description is obtained for the near-contact motion of a particle towards a planar boundary. Convenient formulae are available for F_{VDW} (Gregory 1981; Czarnecki 1979), and F_{ESR} (Hogg, Healy & Fuerstenau 1966).

This work was supported by NASA grant NAG8-945. The authors are very grateful to Professors Huan Jang Keh and Fong Ru Yang for generously providing their collocation source code.

REFERENCES

ACRIVOS, A., JEFFREY, D. J. & SAVILLE, D. A. 1990 Particle migration in suspensions by thermocapillary or electrophoretic motion. *J. Fluid Mech.* **212**, 95–110.

BATCHELOR, G. K. 1982 Sedimentation in a dilute polydisperse system of interacting spheres. Part 1. General theory. *J. Fluid Mech.* **119**, 379–408.

BIKE, S. G. & PRIEVE, D. C. 1990 Electrohydrodynamic lubrication with thin double layers. *J. Colloid Interface Sci.* **136**, 95–112.

BRENNER, H. 1961 The slow motion of a sphere through a viscous fluid towards a plane interface. *Chem. Engng Sci.* **16**, 242–251.

CHEN, S. B. & KEH, H. J. 1988 Electrophoresis in a dilute dispersion of colloidal spheres. *AIChE J.* **34**, 1075–1085.

COOLEY, M. D. A. & O'NEILL, M. E. 1969*a* On the slow motion generated in a viscous fluid by the approach of a sphere to a plane wall or stationary sphere. *Mathematika* **16**, 37–49.

COOLEY, M. D. A. & O'NEILL, M. E. 1969*b* On the slow motion of two spheres in contact along their line of centres through a viscous fluid. *Proc. Camb. Phil. Soc.* **66**, 407–415.

COX, R. G. & BRENNER, H. 1967 The slow motion of a sphere through a viscous fluid towards a plane surface. II. Small gap widths, including inertial effects. *Chem. Engng Sci.* **22**, 1753–1777.

CZARNECKI, J. 1979 van der Waals attraction energy between sphere and half-space. *J. Colloid Interface Sci.* **72**, 361–362.

DAGAN, Z., PFEFFER, R. & WEINBAUM, S. 1982 Axisymmetric stagnation flow of a spherical particle near a finite planar surface at zero Reynolds number. *J. Fluid Mech.* **122**, 273–294.

DAVIS, A. M. J., O'NEILL, M. E., DORREPAAL, J. M. & RANGER, K. B. 1976 Separation from the surface of two equal spheres in Stokes flow. *J. Fluid Mech.* **77**, 625–644.

DAVIS, R. H. 1984 The rate of coagulation of a dilute polydisperse system of sedimenting spheres. *J. Fluid Mech.* **145**, 179–199.

DUKHIN, S. S. & DERAJAGUIN, B. V. 1974 Electrokinetic phenomena. In *Surface and Colloid Science*, vol. 7. Wiley.

ERDELYI, A., MAGNUS, W., OBERHETTINGER, F. & TRICOMI, F. G. 1954 *Tables of Integral Transforms*, vol. II. McGraw-Hill.

GLUCKMAN, M. J., PFEFFER, R. & WEINBAUM, S. 1971 A new technique for treating multiparticle slow viscous flow: axisymmetric flow past spheres and spheroids. *J. Fluid Mech.* **50**, 705–740.

GOREN, S. L. 1970 The normal force exerted by creeping flow on a small sphere touching a plane. *J. Fluid Mech.* **41**, 619–625.

GREGORY, J. 1981 Approximate expressions for retarded van der Waals interaction. *J. Colloid Interface Sci.* **83**, 138–145.

HAPPEL, J. & BRENNER, H. 1983 *Low Reynolds Number Hydrodynamics*. Martinus Nijhoff.

HOGG, R., HEALY, T. W. & FUERSTENAU, D. W. 1966 Mutual coagulation of colloidal dispersions. *Trans. Faraday Soc.* **62**, 1638–1651.

KEH, H. J. & ANDERSON, J. L. 1985 Boundary effects on electrophoretic motion of colloidal spheres. *J. Fluid Mech.* **153**, 417–439.

KEH, H. J. & CHEN, S. B. 1989 Particle interactions in electrophoresis I. Motion of two spheres along their line of centers. *J. Colloid Interface Sci.* **130**, 542–555.

KEH, H. J. & LIEN, L. C. 1989 Electrophoresis of a dielectric sphere normal to a large conducting plane. *J. Chinese Inst. Chem. Engng* **20**, 283.

KEH, H. J. & LIEN, L. C. 1991 Electrophoresis of a colloidal sphere along the axis of a circular orifice or a circular disk. *J. Fluid Mech.* **224**, 305–333.

KEH, H. J. & YANG, F. R. 1990 Particle interactions in electrophoresis. III. Axisymmetric motion of multiple spheres. *J. Colloid Interface Sci.* **139**, 105–116.

KIM, S. & KARRILA, S. 1991 *Microhydrodynamics: Principles and Selected Applications*. Butterworth-Heinemann.

LOEWENBERG, M. & DAVIS, R. H. 1993*a* Near-contact thermocapillary motion of two non-conducting drops. *J. Fluid Mech.* **256**, 107–131.

LOEWENBERG, M. & DAVIS, R. H. 1993*b* Near-contact thermocapillary migration of a non-conducting, viscous drop normal to a plane interface. *J. Colloid Interface Sci.* **160**, 265–275.

MAUDE, A. D. 1961 End effects in a falling-sphere viscometer. *R. J. Appl. Phys.* **12**, 293–295.

MOON, P. & SPENCER, D. E. 1961 *Field Theory Handbook*, p. 104. Springer.

NICHOLS, C. S., LOEWENBERG, M. & DAVIS, R. H. 1995 Electrophoretic particle aggregation. *J. Colloid Interface Sci.* (in review).

O'BRIEN, R. W. 1983 The solution of the electrokinetic equations for colloidal particles with thin double layers. *J. Colloid Interface Sci.* **92**, 204–216.

REED, L. D. & MORRISON, F. A. 1976 Hydrodynamic interaction in electrophoresis. *J. Colloid Interface Sci.* **54**, 117–133.

RUSSEL, W. B., SAVILLE, D. A. & SCHOWALTER, W. R. 1989 *Colloidal Dispersions*. Cambridge University Press.

SMOLUCHOWSKI, M. VON 1903 Contribution à la théorie de l'endosmose électrique et de quelques phenomènes corrélatifs. *Bull. Int. Acad. Sci. Cracovie* **8**, 182–200.

STIMSON, M. & JEFFERY, G. B. 1926 The motion of two spheres in a viscous fluid. *Proc. R. Soc. Lond.* A **111**, 110–116.

TAKAGI, H. 1974 The force on a sphere lying near a plane surface of a viscous fluid. *J. Phys. Soc. Japan* **36**, 1471–1473.

YIANTSIOS, S. G. & DAVIS, R. H. 1991 Close approach and deformation of two viscous drops due to gravity and van der Waals forces. *J. Colloid Interface Sci.* **144**, 412–433.